ACS APPLIED MATERIALS & INTERFACES

Research Article

www.acsami.org

Monolithic Space-Filling Porous Materials from Engineering Plastics by Thermally Induced Phase Separation

Ahmed Elhaj and Knut Irgum*

Department of Chemistry, Umeå University, S-90187 Umeå, Sweden

ABSTRACT: Six different uncompounded engineering and commodity polymers were evaluated for their ability to produce space-filling monolithic entities by thermally induced phase separation (TIPS) from 22 different solvents. Attempts were first made to dissolve the polymers at elevated temperatures, selected below the boiling point of each solvent. Then the solutions of polymers that were homogeneous dissolved underwent a controlled temperature decrease to induce a phase separation as the upper critical solution temperature was passed. Twelve of the solvents gave monolithic entities by this procedure, materials that were characterized with regard to their specific surface area and pore size distribution. These measured parameters were then correlated with their macroporous morphology, assessed by scanning electron microscopy. Monolithic materials with widely different mesoporous properties were obtained with specific surface areas ranging from 169 m^2/g to structures with essentially nonporous skeletons and distinct mesopore size distribution modes from 6 to 15 nm. The materials furthermore had a wide variation in their macroporous morphologies—among the same polymer processed in different solvents and between different polymers dissolved in the same solvent. TIPS processing therefore appears to be a viable route to prepare space-filling meso- and macroporous support materials for a wide variety of purposes in separation science and heterogeneous chemistry.

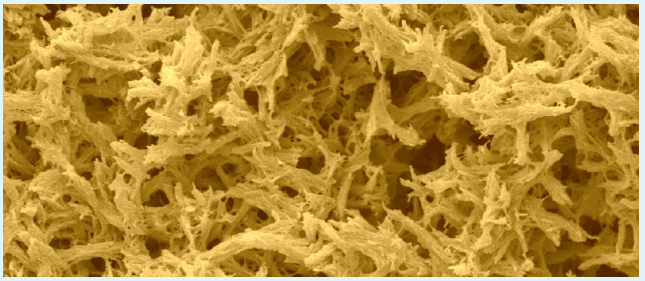

KEYWORDS: *monolithic supports, polymeric scaffolds, heterogeneous chemistry, separation science, thermally induced phase separation*

INTRODUCTION

Since their introduction more than 2 decades ago,[1] macroporous organic monolithic polymers have gained growing interest as versatile support materials in chromatographic separations, in bioseparations, as carriers for (bio)catalysts, and in other flow-through systems[2−5] and also as scaffolds for tissue engineering and other biomedical purposes.[6−8] The key property of porous monoliths aimed at use in separations and as reaction supports is fast mass transfer between the mobile carrier and the support phase. For small molecules, a sufficient surface area is also necessary to provide sites where the interfacial processes can take place. In packed beds the convective flow is supported by the interstitial space, whereas the surface area is provided by a system of mesopores pervading the support, in which the mass transfer is predominantly diffusive. Monolithic materials, being continuous entities, need to provide a bimodal pore system that supports both the convective and diffusive processes and should hence consist of a mesoporous skeleton structure interlaced by a highly interconnected channel network made up of evenly spaced macropores. The bimodal pore system required in monolithic support materials is therefore divided into two groups: micrometer-sized (or larger) pores capable of supporting a percolative flow, and smaller nanometer-sized pores supporting diffusive transport of small solutes into and out of the monolith skeleton.[1] The nanometer-sized pores are further classified into three size categories defined by their nominal pore diameter according to IUPAC's definition:[9] micropores of <2 nm, mesopores ranging from 2 to 50 nm, and macropores of >50 nm. Micropores are usually considered problematic, since their access is limited and interactive processes taking place in such confined spaces are complicated. The pores needed to support efficient diffusive mass transfer and sufficient surface area are therefore mesopores, typically in the range 6−30 nm depending on the size of the entities attached to the carrier surface and on the gyration radius of the molecules that should gain access to those entities.[1]

The most common way of preparing porous organic monoliths is by a one-pot polymerization of mono- and oligovinylic monomers in the presence of a mixture of intermediate/good solvents in the mold where it is finally going to be utilized. The final monolith will therefore have a space-filling shape optimal for the intended use.[1] The porogens are solvents that do not participate in the polymerization reaction, chosen for their ability to promote formation of different parts of the pore system during polymerization. The combined effects of molecular weight increase and cross-linking lead to phase separation of the polymer and the porogens, whereby the polymer precipitates to form a reticulated network. Following removal of the porogens, the cross-linked polymer

Received: March 10, 2014
Accepted: July 2, 2014
Published: July 2, 2014

   dx.doi.org/10.1021/am502977z | *ACS Appl. Mater. Interfaces* 2014, 6, 15653−15666

should ideally comprise an interconnected three-dimensional structure with a pervasive pore system.[1]

Alternatives to chain polymerization of vinylic monomers have also been investigated, such as ring-opening metathesis[10,11] and polycondensation of epoxide/amine[5,12,13] and urea/formaldehyde[14] systems. In a previous communication we have demonstrated a quite different route to monolithic polymers, namely, by thermally induced phase separation (TIPS) of ready-made polymers, which have been dissolved above their upper critical solution temperature (UCST) and allowed to cool to induce a phase separation as the UCST is crossed. By this route, we have been able to prepare macroporous monoliths from several commercially available linear polyamides of different composition.[3,4]

Controlled precipitation of polymers dissolved in good solvents is a methodology that has been used since the 1960s to prepare synthetic membranes for a variety of purposes[15] from commodity plastics such as polypropylene [PP],[16−18] polyamides [PA],[19,20] and polycarbonates [PC],[16,17] as well as from engineering polymers, e.g., poly(vinylidine difluoride) [PVDF],[21−23] polysulfone [PSU],[24] poly(ether sulfone) [PESU],[25−30] poly(phenyl sulfone) [PPSU],[31] and poly(phenylene sulfide) [PPS].[32] The approach first used to establish conditions required for phase separation is nonsolvent induced phase separation (NIPS),[33,34] which is based on dissolving a non-cross-linked polymer in one or several good and/or intermediate solvent(s), casting the polymer solution (called a dope) into a thin film, and thereafter altering the solvent properties of the diluent. This can be done either by selectively removing the good and more volatile member of a solvent pair by evaporation or by diluting the good solvent in the dope film by direct immersion into a miscible nonsolvent, alternatively by letting such a solvent condense onto the film from the gas phase.[3] Substantial efforts have been made to find polymers and solvents for preparing dopes and in adjusting the concentrations, casting temperatures, and precipitation conditions to form porous membranes with tailor-made properties suitable for the intended applications.

Alongside NIPS, thermally induced phase separation (TIPS) has in recent years gained increasing interest as a less elaborate process for producing porous membranes for separation purposes.[15−17,22,23,35−40] The TIPS process is particularly applicable to polymers with high solvent resistance that are difficult to dissolve at room temperature. In the TIPS scheme, the porous membrane structure is established by dissolving the polymer in a good solvent at a temperature above UCST, where the well mixed and clear polymer−solvent solution is thermally quenched by cooling.[16,17,21−23,36,39,40] The total porosity and the size, structure, and distributions of pores in membranes prepared by the TIPS approach are adjustable by manipulating a variety of parameters during the casting such as the polymer composition,[41] conformation,[15,42−44] molecular weight[45−48] and concentration,[15,49,50] selection of diluent (solvent),[51−56] the temperature[57−61] and duration[3,62] of the dissolution, and the quenching temperature[52,63−65] and cooling rate[66−68] of the precipitation step. In spite of the numerous parameters that affect the pore formation, the TIPS technique owns advantages compared to other membrane preparation techniques.[23] Furthermore, since no transfer of matter is involved in the precipitation process, TIPS lends itself to preparation of porous entities in closed molds, which is not possible with a NIPS scheme since exchange of solvents is implicit. Although the seminal description of a TIPS process for forming porous entities via thermal dissolution/precipitation in a patent by Castro[69] covers "forms ranging from films to blocks and intricate shapes", practically all subsequent work employing the TIPS principle has focused on the preparation of thin, porous membranes. As a follow-up to our previous papers describing preparation of sizable porous monoliths made from polyamides by the TIPS route,[3−5] we here describe the formation of similarly sized porous monolithic supports from a variety of commodity plastics and engineering polymers following the TIPS principle.

EXPERIMENTAL SECTION

Materials and Reagents. The polymers used in this work were two different poly(ether sulfone) [PESU] specimens (Ultrason E2020PSRMICRO powder and Ultrason E2020P flakes, both intended for use in solvent based processes), three different grades of poly(sulfone) [PSU] (Ultrason S2010 of " low viscosity", S3010 of "medium viscosity", and S6010 of "high molecular weight" grade), a poly(phenyl sulfone) [PPSU] (Ultrason P3010 of "medium viscosity" grade), and two different grades of poly(butylene terephthalate) [PBT] (Ultradur B2550 of "low viscosity" and B6550 of "high viscosity" grades), all obtained as gifts from BASF (Ludwigshafen, Germany). The source of poly(ethylene terephthalate) [PET] was flakes cut from a 500 mL beverage (incidentally "Coca Cola") bottle, while the poly(ethylene) was sourced from transparent plastic bags made from axially oriented HD-PE film, both of unknown origin and acquired in local supermarkets. The identities of these polymers were identified by Raman spectroscopy (not shown). Structures of the polymers tested are shown in Figure 1.

The solvents (diluents) used in the dissolution studies were *n*-butanol (p.a.) and biphenyl from BDH Chemicals (Poole, England), 1,3-dioxolan-2-one (ethylene carbonate, 98%), cyclohexanone (99.8%), *n*-butyl butyrate (98%), dimethyl succinate, γ-butyrolactone, ε-caprolactone, 1,1,2-trichloroethane (96%), dimethyl sulfoxide [DMSO] ("dry grade"), benzene, and *m*-cresol ("pure grade") from Sigma-Aldrich (Schnelldorf, Germany), phenol, *tert*-butyl acetate (99%) and methylethylketone (99.5%) from Fluka (Buchs, Switzerland), tetrachloroethylene and 1,4-dimethoxybenzene from Hopkin & Williams (Chadwell Heath, U.K.), *n*-propyl acetate (98%) and *N*,*N*-dimethylacetamide (99%) from Merck (Darmstadt, Germany), 2,5-hexanedione from Riedel-de-Haën (Seelze, Germany), *N*,*N*-dimethylformamide (analytical grade) [DMF] from Fisher Scientific (Leicestershire, U.K.), and tetrahydrofuran (p.a.) [THF] from J. T. Baker (Deventer, Holland). The methanol used for Soxhlet extraction was "pure grade" from Prolabo (Paris, France). All solvents were used as received.

Monolith Preparation. Monolith samples were prepared according to the general principles described by Nguyen et al.[5] and started with transfer of 200−400 mg of polymer into 1 g of solvent in 1.5 mL borosilicate glass vials, which were sealed with PTFE-faced septa and crimp caps. Dissolution of the polymers was then attempted (not all polymers did dissolve) at elevated temperatures, followed by controlled cooling. The polymer sample obtained in the form of powder (Ultrason E2020PSRMICRO) was added to the vial containing the solvent in portions under magnetic stirring with a small stir bar, whereas polymers in the form of flakes (PPSU Ultrason E2020P and pieces of PET bottle), film (HD-PE), or pellets (all remaining samples) were added directly to the solvent without stirring. The suspensions thus prepared were purged with nitrogen gas through a 0.4 mm i.d. syringe for about 1 min to remove most of the oxygen from the samples. The actual dissolution took place by immersing the capped vials for varying periods of time in a sand bath that was placed inside the oven of a Hewlett-Packard (Palo Alto, CA) 5890A gas chromatograph to establish accurate temperature control. The temperature measured over time and at different spots in the sand bath varied ±<5 °C. This temperature variation was mainly due to frequent opening of the oven to carry out the mixing cycles, which consisted of a manual shake for ∼15 s every 30 min in order to

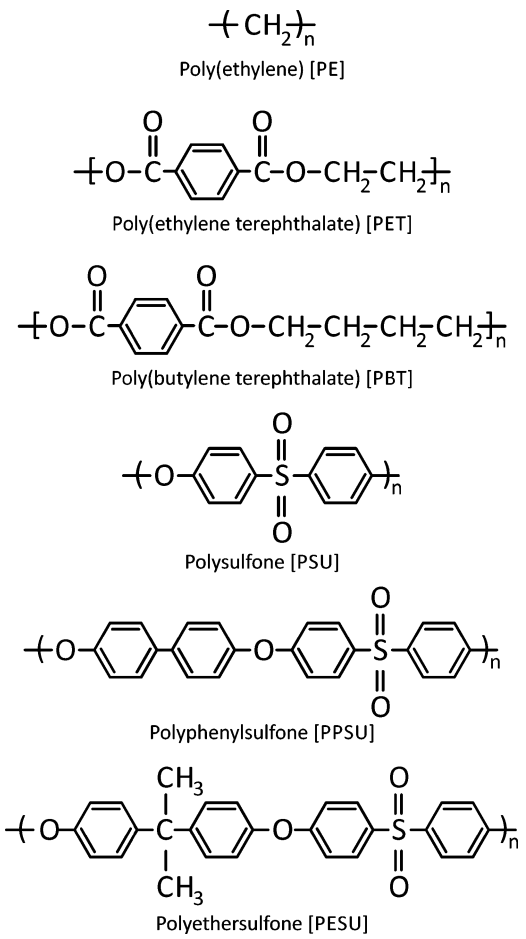

Figure 1. Structures of polymers used in the attempts to prepare monoliths by thermal dissolution/precipitation.

effectuate complete dissolution of the solvent-swollen polymers. When the solutions appeared homogeneous over several shaking cycles, they were left unstirred in the sand bath under continued heating for ~2 h to ascertain complete dissolution. They were thereafter allowed to cool slowly to room temperature with the vials still submersed in the sand bath, at a cooling rate of −0.2 K/min controlled by the temperature programming facility of the 5890A gas chromatograph. The scouting experiments were run at different heating temperatures and times depending on the solvent boiling point, with the maximum temperature used for the dissolution for each polymer/solvent pair listed in Table 1.

After cooling to room temperature, the vials were examined and sorted into classes, depending on the appearance of the contents. Vials with material that looked like solids or stiff gels were broken with minimal force to recover the material as intact as possible. Recovered gels or porous solids were cut into roughly cubical pieces with ~2 mm sides prior to solvent removal. The samples prepared as above were placed in cellulose extraction thimbles (10 mm i.d. by 50 mm long) and covered by small wads of superfine quartz glass wool, then subjected to Soxhlet extraction with methanol for 24 h to extract remaining solvents. The monolithic cubes were finally dried under reduced pressure (~100 Pa) in a Gallenkamp (Loughborough, U.K.) vacuum oven at 40 °C overnight.

Permeability Test. Virgin PPSU P3010 pellets (302 mg) were dissolved in 1.2 mL of γ-butyrolactone at 150 °C for 1 h, using an externally driven rotating device to ascertain mixing by continuous tumbling the vial at ~15 rpm. A glass syringe and a 50 mm by 4.6 mm i.d. HPLC column blank made from poly(etheretherketone) [PEEK] were simultaneously preheated to 180 °C. The clear and homogeneous solution of PPSU P3010 in γ-BL was swiftly transferred into the column by means of the syringe. The transfer took place inside a convection oven heated at 150 °C and was finished in about 1 min. The filled column was capped tightly and placed in the GC oven at the dissolution temperature for an additional hour. The oven was then set to cool at a rate of −0.2 °C/min, as above. After reaching room temperature, the column was connected to a Shimadzu (Kyoto, Japan) LC-10ADvp HPLC pump and flushed with methanol at 10 μL/min flow rate for 1 h. The flow rate was then increased in a stepwise manner up to 999 μL/min and then likewise decreased, recording the pack pressure as it stabilized for each increment/decrement. The combined slopes of the ascending and descending curves were used to compute the intrinsic permeability, k, of the monolith bed according to Darcy's law,

$$k = \frac{Q\mu L}{A\Delta P} \quad (1)$$

where Q is the flow rate, μ the viscosity of the fluidic medium (methanol), L the length of the column, A the cross-sectional area of the column, and ΔP the pressure drop. Statistics were computed using R for Windows (R Foundation for Statistical Computing, Wien; http://www.R-project.org), 64 bit, version 3.1.0.

Surface Area and Pore Size Determination. A total of approximately 100−250 mg of dried monolith cubes was placed in dry sample tubes and additionally dried prior to pore characterization at 120 °C (except HD-PE which was dried at 50 °C to avoid drying close to the melting point of the polymer) for at least 3 h under a continuous flow of dry nitrogen gas using a Micrometrics (Atlanta, GA) Smart Prep degassing unit. The dry samples were thereafter subjected to multipoint nitrogen adsorption−desorption on a Micrometrics Tristar 3000 automated gas adsorption analyzer, measuring the specific surface areas of monolithic materials based on the Brunauer−Emmett−Teller (BET) equation[70] and their average pore widths by the Barrett−Joyner−Halenda (BJH) scheme.[71] Since the BET measurements were based on data from the adsorption part of the isotherm and the BJH from the desorption part, the total specific surface area determined by the BET principle is expected to deviate somewhat from the integrated specific surface area in the BJH scheme.

Scanning Electron Microscopy. Samples of fresh fracture surfaces prepared by snapping monolith cubes in liquid nitrogen (to avoid distortion of the surface by mechanical cutting) were placed on sticky carbon foils attached to standard aluminum specimen stubs and coated with a ~20 nm thick gold layer by a combination of sputter coating by an Edwards (Crawley, U.K.) model S150A sputter coating unit and evaporation by a modified Edwards E14 vacuum coating unit, integrating an automatic tilt and rotate device. Microscopic analysis of samples at random positions was made by an S-360iXP SEM (Leica Cambridge Ltd., Cambridge, U.K.) with a LaB_6 emitter operated at 10 kV, 100 pA probe current, and 0 °C tilt angle.

RESULTS AND DISCUSSION

As the aim of this study was to investigate the possibilities of preparing solid porous monolithic entities from non-cross-linked commodity and engineering polymers, we solicited from commercial sources a variety of uncompounded polymers, namely, PESU, PSU, PPSU, and PBT (for structures see Figure 1). In addition, we sourced samples of PET and HD-PE from a local supermarket. For all these polymers, which were in either powder (PESU Ultrason E2020 PSRMICRO), flake/pellet (PESU Ultrason E2020P, PSU, PPSU, PBT, and PET), or film (HD-PE) forms, we attempted to dissolve them in a series of 22 different organic solvents at elevated temperature. The criteria used for solvent selection were that they should cover a diversity of functional groups with different polar interaction properties (hydrogen bond donor/acceptor and dipolar groups) spanning a wide range of Hildebrand solubility parameters[51,72] and be reasonably stable and nonreactive toward the polymers at the processing temperature. The

Table 1. Qualitative Results from the Dissolution/Precipitation Experiments Listed with Hansen Relative Energy Distance Values

	parameter[a]						PESU		PSU			PPSU	PBT		PET	HD-PE
							E2020 P	E2020 PSRμ	S2010	S3010	S6010	P3010	B2550	B6550		
							δ = 22.8			δ = 22.8		δ = 20.6	δ = 20.6		δ = 20.4	δ = 18.1
							δ_D = 18.7			δ_D = 18.7		δ_D = 18.8	δ_D = 18.0		δ_D = 18.2	δ_D = 18.0
							δ_P = 10.5			δ_P = 10.5		δ_P = 4.8	δ_P = 5.6		δ_P = 6.4	δ_P = 0.0
							δ_H = 7.6			δ_H = 7.6		δ_H = 6.8	δ_H = 8.4		δ_H = 6.6	δ_H = 2.0
solvent	δ	δ_D	δ_P	δ_H	V	TD	R_0 = 9.1			R_0 = 9.1		R_0 = 2.9	R_0 = 4.5		R_0 = 5.0	R_0 = 2.0
n-butyl butyrate	16.8	15.6	2.9	5.6	166.7	150	ND	ND	SW	SW	SW	SW	ND	ND	ND	D/P
							1.10			1.27		2.34	1.37		1.27	3.33
tert-butyl acetate[b]	17.2	15.0	3.7	7.6	133.6	90	ND	ND	ND	ND	ND	ND	ND	ND	ND	ND
							1.10			1.31		2.66	1.41		1.40	4.50
n-propyl acetate	17.6	15.3	4.3	7.6	115.3	90	PD	PD	SW	SW	SW	SW	ND	ND	ND	ND
							1.01			1.21		2.44	1.25		1.25	4.44
benzene	18.5	18.4	0.0	2.0	89.4	75	ND	ND	D/G	PD	D/G	D/P	ND	ND	ND	ND
							1.31			1.34		2.36	1.90		1.58	0.40
methyl ethyl ketone	19.1	16.0	9.0	5.1	90.1	75	SW	SW	D/G	D/G	D/G	D/G	ND	ND	ND	ND
							0.67			1.01		2.48	1.38		1.07	5.16
tetrachloroethylene	19.2	18.3	5.7	0.0	101.2	110	ND	ND	SW	ND	SW	SW	ND	ND	ND	D/P
							0.99			1.14		2.39	1.87		1.33	3.04
tetrahydrofuran	19.5	16.8	5.7	8.0	81.7	55	ND	ND	ND	ND	ND	ND	ND	ND	ND	ND
							0.67			0.80		1.47	0.54		0.64	4.31
cyclohexanone	19.6	17.8	6.3	5.1	104.0	140	D/P	D/P	D/G	D/G	D/G	D/P	ND	ND	ND	D/P
							0.57			0.67		1.04	0.75		0.34	3.52
2,5-hexanedione[b]	19.8	17.1	9.0	4.1	103.1	170	D/G	D/G	ND	ND	ND	ND	ND	ND	ND	ND
							0.55			0.84		2.08	1.28		0.84	4.71
dimethyl succinate[c]	20.1	16.4	5.3	10.3	130.8	150	D/P	D/P	D/P	D/P	D/P	SW	ND	ND	ND	ND
							0.82			0.94		2.06	0.83		1.06	5.18
1,1,2-trichloroethane	20.1	18.2	5.3	6.8	92.9	105	D/L	D/L	D/G	D/G	D/G	D/P	SW	SW	ND	D/P
							0.59			0.56		0.45	0.37		0.22	3.58
biphenyl	21.5	21.4	1.0	2.0	154.1	190	ND	D/P	D/P	D/P	D/P	D/P	ND	ND	ND	D/P
							1.35			1.28		2.77	2.31		1.91	3.44
1,4-dimethoxybenzene[b]	21.8	19.2	4.4	9.4	127.7	145	D/P	D/P	D/P	D/P	D/P	D/P	D/P	D/P	PD	D/P
							0.71			0.52		0.95	0.64		0.80	4.47
m-cresol	22.7	18.0	5.1	12.9	104.7	190	D/L	D/L	D/G	D/G	D/G	D/G	D/G	D/G	D/P	ND
							0.85			0.82		2.18	1.01		1.29	6.02
N,*N*-dimethylacetamide	22.8	16.8	11.5	10.2	92.5	150	D/L	D/L	D/G	D/G	D/G	PD	ND	ND	ND	ND
							0.52			0.86		2.94	1.47		1.37	7.16
n-butanol	23.2	16.0	5.7	15.8	91.5	105	ND	ND	ND	ND	ND	ND	ND	ND	ND	ND
							1.20			1.36		3.67	1.87		2.04	7.73
phenol	24.1	18.0	5.9	14.9	87.5	150	D/L	D/L	D/L	D/P	D/P	D/L	D/P*	D/P*	D/P	ND
							0.96			0.98		2.87	1.45		1.66	7.09
N,*N*-dimethylformamide	24.9	17.4	13.7	11.3	77.0	140	D/L	D/L	D/G	D/L	D/L	PD	ND	ND	ND	ND
							0.61			0.96		3.57	1.93		1.77	8.30

dx.doi.org/10.1021/am502977z | ACS Appl. Mater. Interfaces 2014, 6, 15653−15666

Table 1. continued

solvent	parameter[a] δ	δ_D	δ_P	δ_H	V	TD	PESU E2020 P	PESU E2020 PSRμ	PSU S2010	PSU S3010	PSU S6010	PPSU P3010	PBT B2550	PBT B6550	PET	HD-PE
							δ = 22.8			δ = 22.8		δ = 20.6	δ = 20.6		δ = 20.4	δ = 18.1
							δ_D = 18.7			δ_D = 18.7		δ_D = 18.8	δ_D = 18.0		δ_D = 18.2	δ_D = 18.0
							δ_P = 10.5			δ_P = 10.5		δ_P = 4.8	δ_P = 5.6		δ_P = 6.4	δ_P = 0.0
							δ_H = 7.6			δ_H = 7.6		δ_H = 6.8	δ_H = 8.4		δ_H = 6.6	δ_H = 2.0
							R_0 = 9.1			R_0 = 9.1		R_0 = 2.9	R_0 = 4.5		R_0 = 5.0	R_0 = 2.0
ε-caprolactone	25.8	19.7	15.0	7.4	110.8	170	D/G	D/L	D/G	D/G	D/G	D/P	D/P	D/P	D/P	SW
							0.54			0.85		3.58	2.23		1.83	8.15
γ-butyrolactone	26.3	19.0	16.6	7.4	76.8	150	D/P*	D/L	D/G	D/G	D/G	D/P	ND	ND	ND	ND
							0.67			1.06		4.08	2.49		2.07	8.79
dimethyl sulfoxide	26.7	18.4	16.4	10.2	71.3	150	D/L	D/L	D/G	D/G	D/G	PD	ND	ND	ND	ND
							0.71			1.09		4.18	2.44		2.13	9.18
1,3-dioxolan-2-one	29.6	19.4	21.7	5.1	66.0	150	D/G	D/G	SW	SW	SW	SW	ND	ND	ND	ND
							1.27			1.72		5.87	3.70		3.11	11.05

[a] δ is the Hildebrand solubility parameter, and δ_D, δ_P, and δ_H are the Hansen dispersion, polar, and hydrogen bonding cohesion parameters, all given in units of $MPa^{1/2}$. V is the molecular volume in cm^3/mol. TD is the dissolution temperature in °C, and R_0 is the interaction radius, which divided by the calculated solubility parameter distance, R_a, yields the tabulated RED (relative energy distance) values, all according to ref 77. Listed with the RED values are qualitative outcomes of the dissolution/cooling experiments, coded as ND = not dissolved; SW = swollen but not dissolved; PD = partly dissolved; D = dissolved to form a clear solution, which is combined with L = remained a liquid; G = formed a gel; P = formed a rigid precipitate after cooling. [b] Hansen solubility parameters for *tert*-butyl acetate, 2,5-hexanedione, and 1,4-dimethoxybenzene are lacking in the literature, so data for *sec*-butyl acetate, 2,4-pentanedione, and 1,2-dimethoxybenzene were used instead. All of the Hansen solubility parameter data are from ref 77 except for entries denoted with footnote c. [c] Hansen solubility data are from ref 87. The listed Hildebrand solubility parameters are calculated from the Hansen parameters, according to eq 3.

dx.doi.org/10.1021/am502977z | ACS Appl. Mater. Interfaces 2014, 6, 15653−15666

solvent "line-up" used in the scouting experiments was *n*-butanol, *n*-propyl acetate, *n*-butyl butyrate, *tert*-butyl acetate, dimethyl succinate, 1,3-dioxolan-2-one, methyl ethyl ketone, cyclohexanone, 2,5-hexanedione, dimethyl sulfoxide, *N*,*N*-dimethylformamide, *N*,*N*-dimethylacetamide, γ-butyrolactone, ε-caprolactone, 1,1,2-trichloroethane, tetrachloroethylene, THF, 1,4-dimethoxybenzene, benzene, phenol, *m*-cresol, and biphenyl. Since the foreseen application areas of monoliths resulting from these experiments are as supports for various separation purposes and heterogeneous reaction schemes, the specific surface areas and the macroporous morphologies were the two factors that were primarily taken into account in the evaluation of the prepared monoliths.

Dissolution/Precipitation. Since the formation of monolithic structures by TIPS is a nonequilibrium process,[73] the temperature had to be controlled at a slow decreasing rate to obtain sizable monolithic objects with even pore size distribution.[3] This had the advantage of producing macropores that were large compared to the pores normally seen in TIPS membranes, since slower cooling rates typically result in comparatively larger structural elements,[36,73] evident in the materials produced in our experiments. In most membrane preparations, a macromorphology consisting only of pores in the micrometer range is usually undesirable; yet to allow convective transport in thicker layers as in the applications foreseen for monoliths prepared by the scheme outlined here, through-pores in the micrometer range produced by these experiments are instead advantageous. In terms of uniformity of the mesopores and distribution of macropores, it is obvious that the curing conditions employed in this wide set of scouting experiments were inadequate for many of the polymer/solvent combinations. However, a sufficient number of the structures obtained show morphological features that are highly interesting for use as monolithic sorbents and could serve as a basis for adjustments of the processing conditions in future work.

Initial experiments showed that the process of testing the dissolution/precipitation properties of this polymer/solvent matrix was not as straightforward as expected. After a set of "scouting" experiments intended to identify appropriate conditions, a revised set of experiments was conducted with addition of the powdery PVDF polymer to the solvents under magnetic stirring to avoid formation of lumps and with the dissolution temperatures better adapted with regard to the boiling point for each solvent and to the UCST of each polymer/solvent mixture, based on findings from the initial scouting. The experiments were also designed to allow improved automatic controlled cooling of the polymer/solvent mixtures by means of the temperature programming capabilities of the HP5890 oven. The qualitative outcome of this second set of dissolution/precipitation experiments is listed in Table 1, showing whether the polymers could be fully dissolved in each of the tested solvents and, when clear solutions were obtained, whether the polymers after cooling had solidified as an opaque monolithic structure, formed a clear or slightly milky gel (defined as absence of flow when the vial was tilted), or remained a viscous solution.

The solvents capable of accomplishing a structural transformation of the tested polymers into monolithic entities spanned the entire range of Hildebrand solubility parameters, δ, of solvents tested, from *n*-butyl butyrate (16.8 $MPa^{1/2}$) to 1,3-dioxolan-2-one (29.6 $MPa^{1/2}$). The Hildebrand solubility parameter is a classical measure of solvent strength, which is defined as the square root of the cohesive energy density, i.e., the energy needed per unit volume to break all intermolecular connections in a material;

$$\delta = \sqrt{\frac{\Delta H_{vap} - RT}{V_m}} \quad (2)$$

where ΔH_{vap} is the enthalpy of vaporization, R the gas constant, T the absolute temperature, and V_m the molar volume.[51,72] The Hildebrand solubility parameter can be applied to solvents as well as polymers, and according to the Flory–Huggins solubility theory for macromolecules,[74] a close match is usually required between the solubility parameters of the polymer to be dissolved and a ("good") solvent that is capable of accomplishing its dissolution.

However, the relevance of the Hildebrand parameter proved to be quite limited in this setting, which is evident from Table 1. The best predictions were found for PESU (δ = 22.8), where all the solvents with reasonably close match in Hildebrand parameter (±3 $MPa^{1/2}$) dissolved the polymer. Most of these solutions failed to precipitate, except when cyclohexanone (δ = 19.6), dimethyl succinate (20.1), and 1,4-dimethoxybenzene (21.8) were used as solvents. Several solvents with substantially higher δ values dissolved PESU, including 1,3-dioxalan-2-one which has the highest δ of the solvent set. Also for PSU we note that solvents with δ values higher than that of the polymer generally failed to produce a precipitate after cooling, whereas solvents with lower δ values almost invariably gave monolithic precipitates when solutions were formed. The Hildebrand parameter had a much harder time predicting the solubility of PPSU (δ = 20.6). It was soluble and formed monolithic precipitates in solvents ranging from benzene (δ = 18.5) to γ-butyrolactone (26.3). For PBT (δ = 20.6), solvents with δ values lower than the polymer invariable failed to dissolve the polymer, whereas solutions forming monolithic precipitates could be found all the way up to ε-caprolactone (δ = 25.8). A similar pattern was seen for PET. None of the solvents that were capable of dissolving PBT and PET at elevated temperature were capable of keeping them in solution after cooling, which is in sharp contrast to the three sulfone polymers. Among the solvents, *n*-butanol was clearly an outlier, since it did not dissolve any of the polymers, in spite of its δ being only 0.4 $MPa^{1/2}$ higher than that of PESU and PSU.

The reason for these discrepancies is most probably that the list of solvents mainly consists of relatively polar compounds, many of which are also potent hydrogen bond formers, identifiable by their elevated δ_P and δ_H values (vide infra) in Table 1. It is well-known that the Hildebrand solubility parameter alone fails to describe the matching of more polar solvents with polymeric solutes. We will therefore continue the discussion based on Hansen solubility parameters,[75−77] which are based on the same principle but with the components making up the overall cohesive energy density subdivided into dispersion interactions (δ_D), polar interactions (δ_P), and hydrogen bonding (δ_H), such that their Euclidean norm is equal to the Hildebrand solubility parameter, δ,

$$\delta = \sqrt{{\delta_D}^2 + {\delta_P}^2 + {\delta_H}^2} \quad (3)$$

Founded on these, Hansen has devised a way to predict polymer solubility based on a "relative energy distance", RED, calculated as the Euclidian distance between the Hansen solubility parameters of the polymer (p) and solvent (s) with twice the weight given to the difference in dispersion

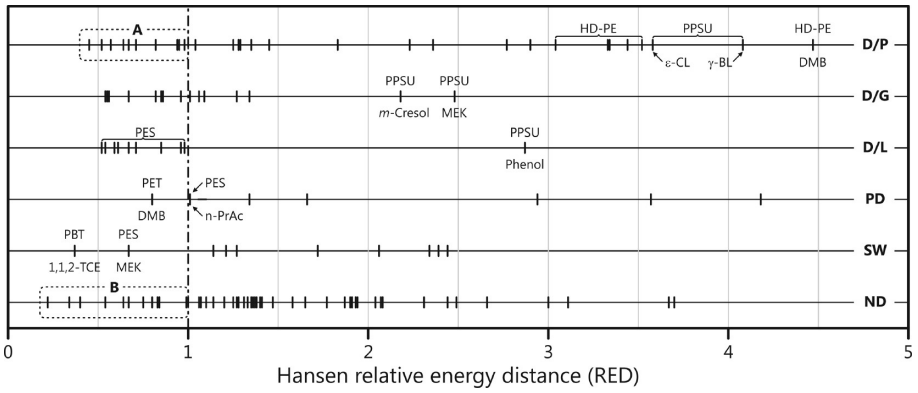

Figure 2. Plot of the Hansen relative energy distance (RED) for the polymer/solvent pairs explored in the survey. The three top entries are experiments where the polymers were fully dissolved and formed a solid precipitate or a gel or remained as a clear viscous liquid after cooling. The three bottom entries are experiments where the polymer did not dissolve as a result of the thermal treatment. For details, see Table 1. Regions in dotted rectangles are polymer/solvent pairs that, according to their Hansen RED values, should have stayed liquid but precipitated (A) or should have dissolved but failed to do so (B). Identifying all polymer solvent pairs would make the plot too crowded, and these entries can instead be located in Table 1.

interactions, δ_D, divided by an "interaction sphere", R_0, which is characteristic of each polymer:[75]

$$\mathrm{RED} = \frac{\sqrt{4(\delta_{D,s} - \delta_{D,p})^2 + (\delta_{P,s} - \delta_{P,p})^2 + (\delta_{H,s} - \delta_{H,s})^2}}{R_0} \quad (4)$$

As a rule of thumb, good solvents for a polymer are found within the "interaction sphere" of the polymer (RED < 1) and bad ones outside this sphere (RED > 1), whereas solvent/polymer pairs with RED values around one are borderline cases.[77] By identification of the contributions to the overall solubility parameter, the idea is that it should be easier to find a good match by using a semiquantitative model describing the "like dissolves like" principle.[78]

However, with few exceptions, tabulated Hansen solubility parameters are related to room temperature. All the contributors to the overall solubility parameter decrease with temperature, especially the hydrogen bonding (δ_H) factor, since hydrogen bonds weaken with increasing temperature. The increase in molar volumes that normally accompanies a temperature increase also causes a decrease in the contribution from polar (δ_P) and dispersive (δ_D) parameters to the overall cohesive energy density of a solvent but to a lesser degree than δ_H. In the set of rather polar solvents used in these experiments, where all solvents except tetrachloroethylene, benzene, and biphenyl have $\delta_P > 5$, the RED concept therefore loses much of its ability to predict whether a polymer will dissolve at elevated temperature. Polymers are typically less affected by these effects than solvents, and their solubility parameters therefore do not decrease to the same extent as those of solvents. A general rule is therefore that hydrogen-bonding solvents turn into better solvents for polymers of lower overall solvent parameters as the temperature increases. A polar solvent that is marginal or bad could therefore become a good solvent at increased temperature by a decrease in its overall solubility parameter, a process that is reversed on cooling. Corrections for temperature can be made by empirical formulas,[77] but this was not done since such extrapolations are based on rather crude approximations and we were mainly interested in the precipitation step of the process, which ultimately ends at room temperature where the predictions should be valid. The Hansen parameters and interaction sphere radii for all diluents and polymers are thus listed in Table 1 and also plotted in Figure 2. For more details on the calculation of RED values, we refer to the most recent edition of Hansen's monography,[77] from which the data used to compute the values were also taken.

When the outcomes of the dissolution experiments are reassessed in view of the Hansen RED values for the solvent/polymer pairs, the results become more rational. We first recall that PESU (δ = 22.8) was successfully dissolved in a wide range of solvents ranging in δ from 19.6 to 29.6. Noticeable is that none of the RED values for these solvent/polymer pairs exceed 1.35, a value that is found for biphenyl, which in spite of having a rather close match in Hildebrand solubility parameter (δ = 21.5) actually failed to dissolve one of the PESU samples tested. Part of the explanation for this wide range of good solvents is the comparatively large interaction spheres, R_0, of PESU and PSU (9.1) which yield comparatively low RED values according to eq 4. In effect this means that PESU and PSU are less "picky" in the choice of good solvents compared to, for example, HD-PE. All these solvent are within or only slightly outside the interaction spheres of their polymers, and the Hansen solubility parameters therefore predict that these solutions should be stable.

It is clear that the RED values can give some guidance, but there are also some significant mispredictions, which are found in the regions indicated by dotted lines in Figure 2. Both regions consist of polymer/solvent pairs where the RED values indicate dissolution. In region A the polymers dissolved but produced a solid precipitate in spite of RED values of <1. This region is populated by all polymers except PET and HD-PE, which only a few of the solvents tested were capable of dissolving. PPSU P3010 produced clear solutions and yielded monolithic structures from 1,1,2-trichloroethane (RED = 0.45) and 1,4-dimethoxybenzene (0.95); PSU from *p*-DMB (0.52), dimethylsuccinate (0.94), and phenol (0.98); PESU from cyclohexanol (0.57) and from dimethylsuccinate (0.82); PBT from 1,4-dimethoxybenzene (0.64). At the opposite end of the RED scale of polymers that dissolved and formed monolith-like precipitates (D/P), we find PPSU in combination with biphenyl (2.77), ϵ-caprolactone (3.58), and γ-butyrolactone (4.08). Clearly the RED values predict that these solvents

should not dissolve PPSU, yet a scrutiny of the contributors to the overall solubility parameter reveals that there is a rather close match in δ_D (18.8 for PPSU and 19.0 and 19.7 for γ-butyrolactone and ε-caprolactone, respectively). The decreased contribution from polar interactions at 150−170 °C apparently made the match in overall solubility parameters sufficiently close for dissolution to take place, in spite of the relatively large RED values. Even more surprising was that PPSU remained in solution following its dissolution in phenol, as the RED value of this polymer/solvent pair is 2.87.

The other polymer found in the upper part of the RED scale in the D/P category is HD-PE, where the RED values for all solvents capable of dissolving the polymer were consistently above 3. The notable exception is benzene, the only solvent actually inside the interaction sphere of HD-PE, which failed to dissolve the polymer. This could be connected to a lower processing temperature, dictated by the boiling point of benzene. None of the solvents that actually dissolved HD-PE should therefore be really well suited for processing this polymer; still it dissolved in tetrachloroethylene (RED = 3.04; TD = 110 °C), *n*-butyl butyrate (3.33; 150 °C), biphenyl (3.44; 190 °C), cyclohexanone (3.52; 140 °C), 1,1,2-trichloroethane (3.58; 105 °C), and 1,4-dimethoxybenzene (4.47; 145 °C), producing monolithic materials with vastly different appearances, as illustrated in Figure 3. Yet none of these HD-PE monolithic entities showed specific surface areas by N_2 cryosorption (Table 2) that indicate a significant porosity except the external surfaces of their macroreticular network. The material processed in tetrachloroethylene at 110 °C shows signs of a melting process with long drawn-out strings, whereas the other solvents gave more lamellar structures. These dissolution temperatures range from just below to above the melting point range of polyethylene (120−180 °C depending on crystalline structure), so we suspect that the formation of a monolith-like network could in some cases have followed a melting route than true dissolution. Still, these solutions had an entirely clear appearance in the hot state.

The region marked as B in Figure 2 are polymers that did not dissolve, although their RED values are below the "critical" limit of 1. The closest solvation parameter matches were seen for PET in 1,1,2-trichloroethane (RED = 0.22) and cyclohexanone (0.34), but also THF (0.64), 1,4-dimethoxybenzene (0.80), and 2,5-hexadione (0.84) were well inside the "interaction sphere" of PET and still unable to dissolve the polymer. However, since the PET was sampled from a locally obtained beverage bottle, the polymer has an uncertain composition, and it is known that isophthalic acid, diethylene glycol, cyclohexane dimethanol, and other co-monomers are regularly used in the production of PET bottles.[79] Yet cross-linking should not be a cause of this failure to dissolve in spite of favorable RED values, since *m*-cresol (1.29) and ε-caprolactone (1.83) produced clear solutions. However, a "reactive dissolution" by alcoholysis or transesterification cannot be completely excluded, since these solvents are phenolic compound and a cyclic ester. Such depolymerization reactions are encountered for instance in recycling of PET by glycolysis, but these reactions call for a metal catalyst which is critical for the success.[80] Contradicting this caveat is the fact that PET gave rigid monolithic structures (Figure 4) after processing in both *m*-cresol and ε-caprolactone. Other entries of significance in the "B region" are the four polymers that failed to dissolve in THF in spite of favorable RED values: PBT (0.54), PET (0.64), PESU (0.67), and PSU

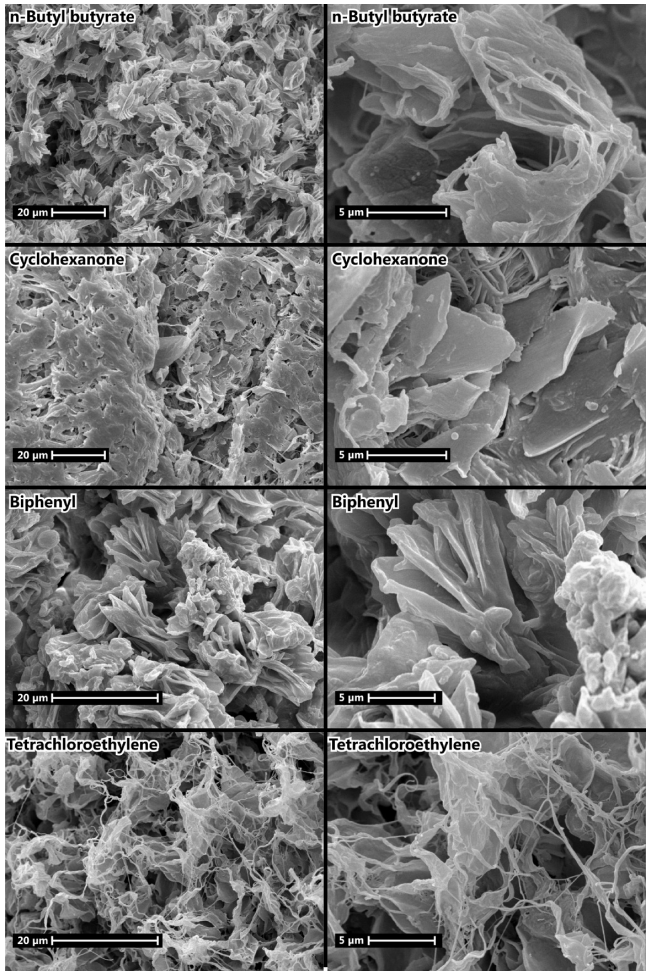

Figure 3. SEM micrographs of random fracture surfaces for monoliths prepared by precipitation of HD-PE from *n*-butyl butyrate, cyclohexanone, biphenyl, and tetrachloroethylene with gradual slow cooling. Images of each sample were acquired at two different magnifications (indicated by scale bars) to illustrate the pore uniformity and skeleton structure.

(0.80). Then again, THF was the solvent that used at the lowest dissolution temperature (55 °C).

A final observation is that PBT of both low (B2550) and high (B6550) viscosity grades dissolved in 1,4-dimethoxybenzene (0.64), phenol (1.45), ε-CL (2.23), and *m*-cresol (1.01), forming monolithic precipitates from the three first solvents mentioned and a gel from *m*-cresol. In most other solvents PBT failed to dissolve. It was therefore somewhat surprising to find that PPSU, whose interaction sphere is substantially smaller (R_0 = 2.9 compared to 4.5 for PBT) actually dissolved in a wider range of solvents (Table 1). The same comparison with PPSU also applies to PET. We also note that monolithic structures were formed in solutions where the Hansen RED values predict solubility (for PPSU in 1,1,2-trichloroethane and for PPSU and PBT in 1,4-dimethoxybenzene) and also that the elevated dissolution temperatures led to formation of polymer solution with solvents well outside their "interaction sphere".

These difficulties of more accurately predicting polymer solubility and whether a polymer that dissolves at elevated temperature will (within the time frame of the experiments conducted here) precipitate, form a gel, or remain as a liquid are most probably related to the difficulties of establishing exact

Table 2. Specific Surface Areas of Monolithic Materials Produced[a]

	PESU		PPSU	PBT			
solvent	E2020 P	E2020 PSRμ	P3010	B2550	B6550	PET	HD-PE
1,1,2-trichloroethane	ND	ND	157 ± 1.0	ND	ND	ND	6.50 ± 0.07
2,5-hexanedione	ND	ND	ND	ND	ND	ND	ND
butyl butyrate	ND	ND	ND	ND	ND	ND	3.31 ± 0.08
cyclohexanone	1.54 ± 0.03	1.25 ± 0.02	87.0 ± 0.50	ND	ND	ND	14.7 ± 0.09
dimethyl succinate	ND	ND	ND	ND	ND	ND	ND
m-cresol	ND	ND	ND	ND	ND	2.60 ± 0.08	ND
1,4-dimethoxybenzene	ND	ND	85.2 ± 0.60	71.3 ± 0.30	77.6 ± 0.30	ND	1.22 ± 0.037
phenol	ND	ND	ND	65.7 ± 0.28	69.4 ± 0.30	1.40 ± 0.02	ND
tetrachloroethylene	ND	ND	ND	ND	ND	ND	7.3 ± 0.09
γ-butyrolactone	0.79 ± 0.02	ND	169 ± 1.0	ND	ND	ND	SW
ε-caprolactone	ND	ND	58.7 ± 0.40	N/M	20.1 ± 0.10	26.6 ± 0.15	ND
biphenyl	ND	2.66 ± 0.06	82.4 ± 0.50	ND	ND	ND	3.04 ± 0.03

[a]Quantitative outcomes are as indicated in Table 1. N/M, not measurable because of negative *c* values in the BET procedure.

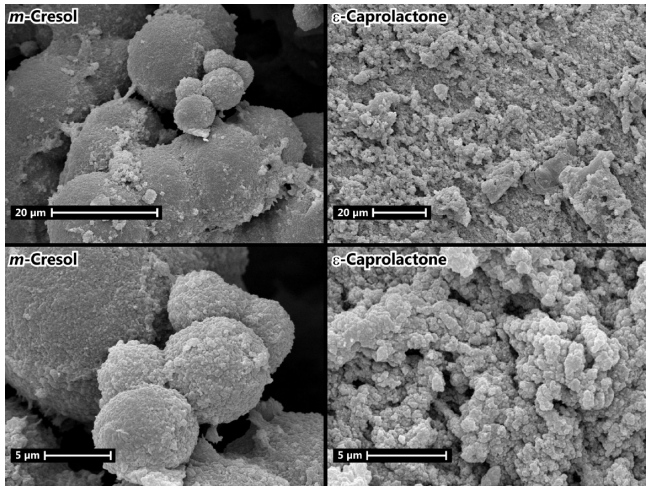

Figure 4. SEM micrographs of random fractures surface areas of monoliths prepared by dissolution/precipitation of PET from *m*-cresol and ε-caprolactone, as indicated in the figure. Note the different scales in the two pairs of images.

values for the solubility parameters of polymers, since their heats of vaporization cannot be determined directly. Tabulated values are therefore determined by swelling, viscosity, or compatibility charts (i.e., qualitative information similar to that provided in Table 1) or have been estimated by group contribution theory.[77] Getting a grip on the exact contribution of hydrogen bonding to solubility parameters of solvents is also tricky, since the contribution of δ_H has to be been determined from δ and empirically estimated values of δ_D and δ_P according to eq 3.[81] The errors in δ_H could therefore be quite substantial. In view of this, the predictability of RED values accounted for above is probably as good as can be expected. The solubility parameters can consequently give us some guidance selecting solvents for polymers to be processed according to the TIPS principle but are unreliable in predicting the exact outcome of the experiments.

Dry State Porous Properties of Recovered Monolithic Entities. Adsorption/desorption of nitrogen gas at cryotemperature is a widely used technique for determination of surface area and distribution of pore sizes of porous substances in the dry state. The technique is useful for characterizing porous substances covering a wide range of pore sizes in the micro- and mesopores range and is applicable for porous solids of all kinds.[70,71,82] Scanning electron microscopy (SEM) yields useful information on the macroporous structure of materials through quasi three-dimensional images with a wide apparent depth of field[83,84] but is of limited use for studying surface morphology at the mesopore level. We therefore made combined use of these techniques to assess the monolithic structures prepared in this work.

Table 2 lists the porous properties of the monolithic material produced by the polymer/solvent combinations marked as dissolved and precipitated (D/P) in Table 1. The most interesting entries in this table are the materials with higher surface areas, namely, PPSU and PBT. The highest specific surface areas were seen for PPSU processed in γ-butyrolactone (169 ± 1 m^2/g) and 1,1,2-trichloroethane (157 ± 1 m^2/g), but also cyclohexanone, biphenyl, ε-caprolactone, and 1,4-dimethoxybenzene produced PPSU monoliths with surface areas in the range 60−80 m^2/g. Samples prepared from PBT also gave BET surface areas in the 60−80 m^2/g range from 1,4-dimethoxybenzene and phenol. For these materials, it was intriguing to see how the surface areas were distributed among pores of different sizes. The cumulative BJH desorption surface areas of the monoliths prepared from PPSU and PBT were therefore plotted against pore size and are presented in Figure 5. In the following section we will discuss these in the context of the corresponding SEM images, which are shown in Figures 6 and 7.

Scanning electron micrographs of monolith prepared from PPSU shown in Figure 6 reveal quite different macroporous morphologies for the materials produced in different solvents. The PPSU processed in γ-butyrolactone not only had the highest surface area among all the tested polymer/solvent combinations (Table 2); this solvent also yielded the narrowest pore size distribution, centered around 6−7 nm. Apparent from the top row in Figure 6 it also produced the most homogeneous material among the PPSU monoliths produced, best characterized as a structure of well-fused spherulites.

PPSU processed in 1,1,2-trichloroethane showed a slightly wider pore size distribution and also a higher fraction of larger pores, centered around 8−9 nm. The macrostructure was rather homogeneous, but as opposed to the γ-butyrolactone sample, there were several interruptions in the structure in the form of cracks. Whether these were originally there or are the result of the drying or SEM sample preparation procedures cannot be determined.

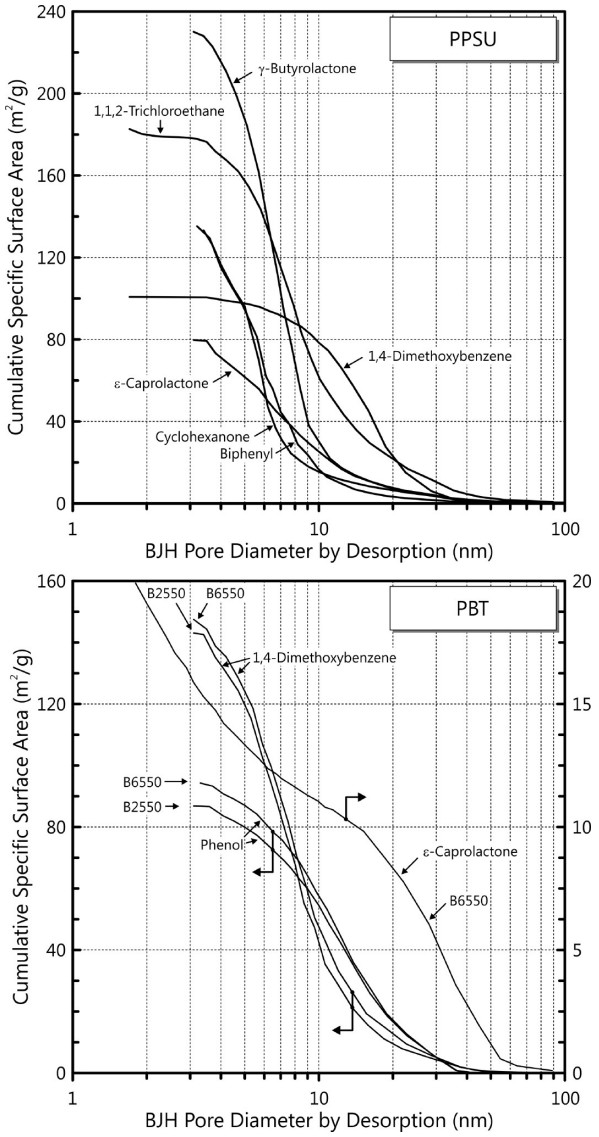

Figure 5. Cumulative distributions of specific surface area across the mesopore range measured by nitrogen desorption according to the BJH principle[71] for PPSU and PBT in the solvents that gave porous monolithic products by thermally induced phase separation. Note that the left ordinates have different scale and the dual scale in the bottom panel.

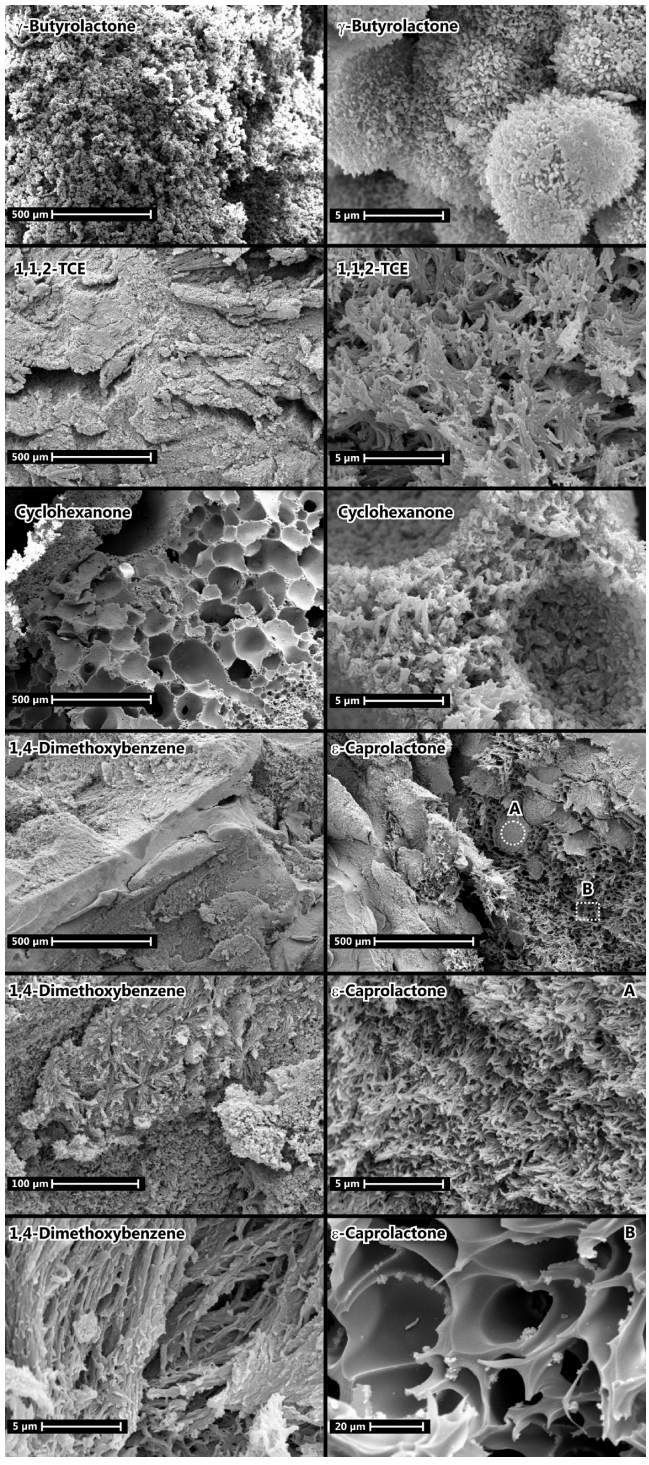

Figure 6. SEM micrographs of random fractures surface areas of monoliths prepared by dissolution/precipitation of PPSU P3010 from γ-butyrolactone, 1,1,2-trichloroethane, and cyclohexanone shown at two different magnifications. The bottom three rows show samples with pronounced heterogeneous macromorphologies prepared from 1,4-dimethoxybenzene and ε-caprolactone, with A and B being magnifications of areas indicated in the uppermost of the ε-caprolactone images.

The PPSU monolith prepared from 1,4-dimethoxybenzene had a lower specific surface area compared to those prepared in γ-butyrolactone and 1,1,2-trichloroethane (85.2 ± 0.6 m^2/g) but instead showed a sharp mode for pores around 15 nm, combined with an almost total absence of smaller mesopores and micropores, as is evident from the top panel of Figure 5. However, judging from the lowest magnification of the corresponding SEM micrograph in Figure 6, the macrostructure seemed rather heterogeneous. Zoomed in, it is apparent that the more ordered part of the PPSU monolithic structure had crystallized into continuous structures composed of aligned axialitic elements that seem to have originated from central spherulites. There were also less ordered regions more resembling a polymer that had undergone solid−liquid phase separation, most evident at the intermediate magnification. Notable is that the samples prepared from γ-butyrolactone, 1,1,2-trichloroethane, and 1,4-dimethoxybenzene showed an almost perfect inverse relationship between specific surface area and pore size mode (plot now shown), from which the monoliths prepared from the remaining solvents deviated.

dx.doi.org/10.1021/am502977z | ACS Appl. Mater. Interfaces 2014, 6, 15653−15666

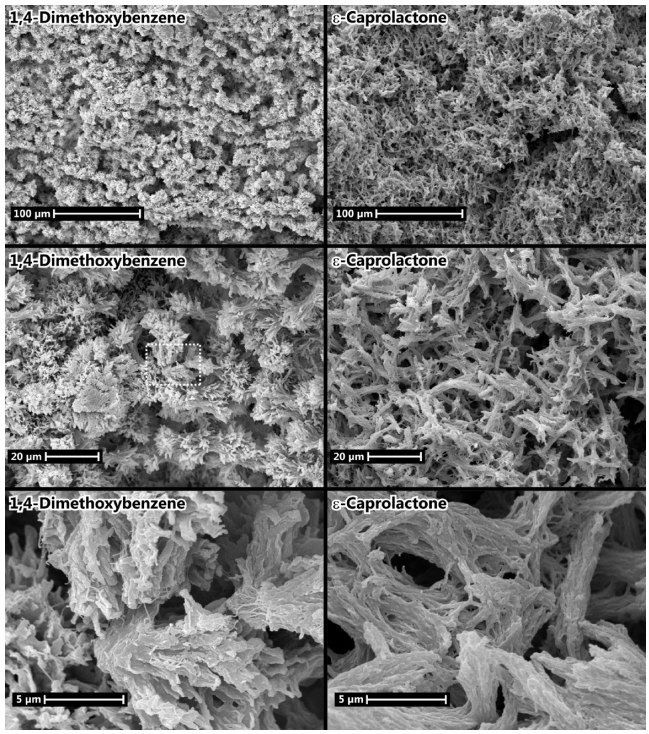

Figure 7. SEM micrographs of random fractures surface areas of monoliths prepared by dissolution/precipitation of PBT B6550 from 1,4-dimethoxybenzene and ε-caprolactone, as indicated in the figure.

The PPSU monoliths processed in cyclohexanone and biphenyl (images not shown) showed shallower pore size distribution curves with modes centered around 5 nm. The material resulting from processing of PPSU in cyclohexanone was radically different from the others with a polyHIPE[85] type macroporous morphology (Figure 6). The connectivity of the spherical voids appears to be low, which is not surprising since a rather high polymer loading of 27.5 wt % was used in this experiment. It is interesting to note that this structure was established without addition of any surface active agent or other structure-directing element, which is common in polyHIPE preparation. The last solvent capable of forming monolithic structures with PPSU was ε-caprolactone, but the material produced by this polymer/solvent combination had no clear mode in its pore size distribution. Both biphenyl and ε-caprolactone produced monoliths with rather similar and pronounced heterogeneous macromorphologies, illustrated by SEM images for ε-caprolactone in Figure 6, with two magnified sections having radically different structures. The region marked as A was composed of well dispersed axialites tapered to needle-like points (this could be an artifact due to sample preparation, in spite of the cryosnapping procedure used), whereas region B consisted of large (~10−30 μm) macropores intersected by precipitated polymer, whose surface appeared to be very smooth also at the highest SEM magnification. Judging from the lowest and middle magnification, the connectivity between these pores seems to be quite limited and the fracture surface seen at the highest magnification reveals that there is a high degree of orientation in the core polymer. This is most likely due to a crystallization-induced orientation of the polymer chains during the precipitation, since PPSU is known to be a highly crystalline polymer.[86] The morphological differences of PPSU P 3010 monolith prepared from the six different solvents that yielded monolithic structures indicate that PPSU monoliths with vastly macro- and mesoporous properties can be prepared simply by choosing different solvents. This makes PPSU an interesting polymer for continued experiments in monolith preparation by TIPS.

Another of the tested polymers that yielded monolithic structures with intriguing morphology from several solvents was PBT. Two samples of different molecular weight were evaluated: B2550 with viscosity number (0.05 g/mL in phenol/1,2-dichlorobenzene) of 107 and B6550 with a viscosity number of 160. The PBT materials prepared from 1,4-dimethoxybenzene showed a sharp mode in their pore size distributions around 8 nm, whereas the materials recovered from phenol had a more shallow mode around 11−12 nm. Interestingly, the two PBT samples of different molecular weight produced practically identical pore size distributions in both these solvents and the SEM images were also very similar. However, the TIPS materials prepared from PBT B2550 in phenol had highly discontinuous broken-up platelike structures that were deemed useless as monolithic supports. Only the monolith prepared from PBT B6550 in 1,4-dimethoxybenzene is therefore shown in Figure 7. This sample had a fused system of evenly spaced and aggregated coral-like entities of about 5−15 μm diameter, with surfaces showing a reticulated structure with some alignment. The third solvent that produced monolithic entities from PBT was ε-caprolactone, although the specific surface area (Table 2) was substantially smaller than that obtained from 1,4-dimethoxybenzene and phenol. The PBT B6550 monolith prepared in ε-caprolactone featured a continuous micrometer-sized network with a more pronounced connected rod character. The polymer segments making up the rods consisted of even smaller, submicrometer rodlike structures that appeared to be largely aligned within each skeleton rod. Nitrogen cryosorption was successful only for the B6550 grade; B2550 gave negative c-values in the BET equation, probably because of excessive micropores. As is seen from the BJH trace for the B6550 samples in Figure 5 (note the different scale), there is a pore diameter mode around 30 nm, but the surface area continues to grow into the micropore region, giving a hint that micropores could be the reason why the B2550 sample was not measurable by the BET scheme.

Finally a permeability test was made to verify the flow-through properties of the monoliths prepared by TIPS. For this, we chose PPSU P3010 processed in γ-butyrolactone, since this was the combination that produced the highest specific surface area. This test was carried out on a monolith molded in a PEEK column, directly after flushing the solvent out of the monolith with methanol, by altering the flow rate of methanol in steps and monitoring the back-pressure. Plots of back-pressure against flow rate were linear and without hysteresis (slopes with standard errors for 95% confidence intervals were 1.90 ± 0.039 and 1.95 ± 0.043 MPa·min·cm^{-3} for the pressure vs flow rate dependencies of the increasing and decreasing data series, respectively, with adjusted r^2 of 0.9979 and 0.9976), and the intrinsic permeability of the monolith was calculated to be 1.48 × 10^{-13} m^2 by Darcy's law (eq 1), using 5.7 × 10^{-1} Pa·s as the dynamic viscosity of methanol at the measurement temperature of 22 °C.[88]

CONCLUSIONS

This scouting work has explored the possibilities of preparing sizable porous monolithic entities from a variety of commodity

and "engineering" polymers, where the focus has been on finding readily available solvents that are capable of dissolving a series of different polymers, to yield monolithic structure when the solutions are subjected to cooling. The most interesting results were obtained from PPSU, PBT, and HD-PE which produced monolithic entities by the TIPS procedure in 12 out of the 22 different solvents tested. The successful solvents belonged predominantly to the categories higher aliphatic esters and ketones, chlorinated hydrocarbons, and aromatic hydrocarbons. PPSU P3010 turned out to be a potential candidate for future studies in terms of the relatively high specific surface areas obtained, whereas PBT, PET, and HD-PE monoliths showed the most homogeneous macrostructures with high uniformity of the pore distribution. The solvent 1,4-dimethoxybenzene was capable of dissolving almost all the polymers. Hansen and in particular Hildebrand solubility parameters had limited utility in predicting the outcome of TIPS experiments, a limitation that can mainly be ascribed to the difficulties of establishing exact interaction parameters for polymers but also to the temperature dependence of these parameters. Overall, the simplicity of the preparation process and the variation in both meso- and macroporous properties that can be obtained by the TIPS procedure make it an attractive alternative way to prepare monolithic supports for separation science and heterogeneous chemistry.

AUTHOR INFORMATION

Corresponding Author

*E-mail: kim@chem.umu.se.

Notes

The authors declare no competing financial interest.

ACKNOWLEDGMENTS

The authors are indebted to BASF for its generous gifts of the polymers used in this work. This work was supported by The Swedish Science Foundation (VR) through Grant 2012-4000.

REFERENCES

(1) Svec, F.; Tennikova, T. B.; Deyl, Z. *Monolithic Materials*; Elsevier: Amsterdam, 2003.

(2) Trilisky, E. I.; Koku, H.; Czymmek, K. J.; Lenhoff, A. M. Relation of Structure to Performance Characteristics of Monolithic and Perfusive Stationary Phases. *J. Chromatogr., A* **2009**, *1216*, 6365−6376.

(3) Nguyen, A. M.; Nordborg, A.; Shchukarev, A.; Irgum, K. Thermally Induced Dissolution/Precipitation—A Simple Approach for the Preparation of Macroporous Monoliths from Linear Aliphatic Polyamides. *J. Sep. Sci.* **2009**, *32*, 2619−2628.

(4) Nguyen, A. M.; Nguyen, T. D.; Irgum, K. Sizeable Macroporous Monolithic Polyamide Entities Prepared in Closed Molds by Thermally Mediated Dissolution and Phase Segregation. *Chem. Mater.* **2008**, *20*, 6244−6247.

(5) Nguyen, A. M.; Irgum, K. Epoxy-Based Monoliths. A Novel Hydrophilic Separation Material for Liquid Chromatography of Biomolecules. *Chem. Mater.* **2006**, *18*, 6308−6315.

(6) Carfi Pavia, F.; La Carrubba, V.; Piccarolo, S.; Brucato, V. Polymeric Scaffolds Prepared via Thermally Induced Phase Separation: Tuning of Structure and Morphology. *J. Biomed. Mater. Res.* **2008**, *86A*, 459−466.

(7) Hsu, S.-H.; Huang, S.; Wang, Y.-C.; Kuo, Y.-C. Novel Nanostructured Biodegradable Polymer Matrices Fabricated by Phase Separation Techniques for Tissue Regeneration. *Acta Biomater.* **2013**, *9*, 6915−6927.

(8) Lu, T.; Li, Y.; Chen, T. Techniques for Fabrication and Construction of Three-Dimensional Scaffolds for Tissue Engineering. *Int. J. Nanomed.* **2013**, *8*, 337−350.

(9) McNaught, A. D., Wilkinson, A., Eds. *IUPAC Compendium of Chemical Terminology*, 2nd ed.; Blackwell Scientific Publications: Oxford, U.K., 1997. Online corrected version: http://goldbook.iupac.org.

(10) Sinner, F. M.; Buchmeiser, M. R. Ring-Opening Metathesis Polymerization: Access to a New Class of Functionalized, Monolithic Stationary Phases for Liquid Chromatography. *Angew. Chem., Int. Ed.* **2000**, *39*, 1433−1436.

(11) Buchmeiser, M. R. Stationary Phases for Chromatography Prepared by Ring Opening Metathesis Polymerization. *J. Sep. Sci.* **2008**, *31*, 1907−1922.

(12) Hosoya, K.; Hira, N.; Yamamoto, K.; Nishimura, M.; Tanaka, N. High-Performance Polymer-Based Monolithic Capillary Column. *Anal. Chem.* **2006**, *78*, 5729−5735.

(13) Tsujioka, N.; Ishizuka, N.; Tanaka, N.; Kubo, T.; Hosoya, K. Well-Controlled 3D Skeletal Epoxy-Based Monoliths Obtained by Polymerization Induced Phase Separation. *J. Polym. Sci., Part A: Polym. Chem.* **2008**, *46*, 3272−3281.

(14) Sun, X.; Chai, Z. Urea−Formaldehyde Resin Monolith as a New Packing Material for Affinity Chromatography. *J. Chromatogr., A* **2002**, *943*, 209−218.

(15) Guillen, G. R.; Pan, Y.; Li, M.; Hoek, E. M. V. Preparation and Characterization of Membranes Formed by Nonsolvent Induced Phase Separation: A Review. *Ind. Eng. Chem. Res.* **2011**, *50*, 3798−3817.

(16) Matsuyama, H.; Kim, M.; Lloyd, D. R. Effect of Extraction and Drying on the Structure of Microporous Polyethylene Membranes Prepared via Thermally Induced Phase Separation. *J. Membr. Sci.* **2002**, *204*, 413−419.

(17) Matsuyama, H.; Okafuji, H.; Maki, T.; Teramoto, M.; Kubota, N. Preparation of Polyethylene Hollow Fiber Membrane via Thermally Induced Phase Separation. *J. Membr. Sci.* **2003**, *223*, 119−126.

(18) Lin, Y. K.; Chen, G.; Yang, J.; Wang, X. L. Formation of Isotactic Polypropylene Membranes with Bicontinuous Structure and Good Strength via Thermally Induced Phase Separation Method. *Desalination* **2009**, *236*, 8−15.

(19) (a) Cheng, L. P.; Dwan, A. W.; Gryte, C. C. Membrane Formation by Isothermal Precipitation in Polyamide-Formic Acid-Water Systems. I. Description of Membrane Morphology. *J. Polym. Sci., Part B: Polym. Phys.* **1995**, *33*, 211−222. (b) Cheng, L. P.; Dwan, A. W.; Gryte, C. C. Membrane Formation by Isothermal Precipitation in Polyamide-Formic Acid-Water Systems. II. Precipitation Dynamics. *J. Polym. Sci., Part B: Polym. Phys.* **1995**, *33*, 223−235.

(20) (a) Bulte, A. M. W.; Mulder, M. H. V.; Smolders, C. A.; Strathmann, H. Diffusion Induced Phase Separation with Crystallizable Nylons. I. Mass Transfer Processes for Nylon 4,6. *J. Membr. Sci.* **1996**, *121*, 37−49. (b) Bulte, A. M. W.; Mulder, M. H. V.; Smolders, C. A.; Strathmann, H. Diffusion Induced Phase Separation with Crystallizable Nylons. II. Relation to Final Membrane Morphology. *J. Membr. Sci.* **1996**, *121*, 51−58.

(21) Gu, M.; Zhang, J.; Wang, X.; Tao, H.; Ge, L. Formation of Poly(vinylidene fluoride) (PVDF) Membranes via Thermally Induced Phase Separation. *Desalination* **2006**, *192*, 160−167.

(22) Gu, M.; Zhang, J.; Xia, Y.; Wang, X. Poly(vinylidene fluoride) Crystallization Behavior and Membrane Structure Formation via Thermally Induced Phase Separation with Benzophenone Diluent. *J. Macromol. Sci., Part B: Phys.* **2008**, *47*, 180−191.

(23) Cui, Z.-Y.; Xu, Y.-Y.; Zhu, L.-P.; Deng, H.-Y.; Wang, J.-Y.; Zhu, B.-K. Preparation of PVDF-HFP Microporous Membranes via the Thermally Induced Phase Separation Process. *J. Macromol. Sci., Part B: Phys.* **2009**, *48*, 41−54.

(24) (a) Radovanovic, P.; Thiel, S. W.; Hwang, S.-T. Formation of Asymmetric Polysulfone Membranes by Immersion Precipitation. Part I. Modelling Mass Transport during Gelation. *J. Membr. Sci.* **1992**, *65*, 213−229. (b) Radovanovic, P.; Thiel, S. W.; Hwang, S.-T. Formation of Asymmetric Polysulfone Membranes by Immersion Precipitation. Part II. The Effects of Casting Solution and Gelation Bath Compositions on Membrane Structure and Skin Formation. *J. Membr. Sci.* **1992**, *65*, 231−246.

(25) Xu, Z.-L.; Alsalhy Qusay, F. Polyethersulfone (PES) Hollow Fiber Ultrafiltration Membranes Prepared by PES/Non-Solvent/NMP Solution. *J. Membr. Sci.* **2004**, *233*, 101−111.
(26) Shin, S.-J.; Kim, J.-P.; Kim, H.-J.; Jeon, J.-H.; Min, B.-R. Preparation and Characterization of Polyethersulfone Microfiltration Membranes by a 2-Methoxyethanol Additive. *Desalination* **2005**, *186*, 1−10.
(27) Laninovic, V. Relationship between Type of Nonsolvent Additive and Properties of Polyethersulfone Membranes. *Desalination* **2005**, *186*, 39−46.
(28) Li, Z.-H.; Jiang, C.-Z. Investigation of the Dynamics of Poly(ether sulfone) Membrane Formation by Immersion Precipitation. *J. Polym. Sci., Part B: Polym. Phys.* **2005**, *43*, 498−510.
(29) Ismail, A. F.; Norida, R.; Abdul Rahman, W. A. W.; Matsuura, T.; Hashemifard, S. A. Preparation and Characterization of Hyperthin-Skinned and High Performances Asymmetric Polyethersulfone Membrane for Gas Separation. *Desalination* **2011**, *273*, 93−104.
(30) Arthanareeswaran, G.; Starov, V. M. Effect of Solvents on Performance of Polyethersulfone Ultrafiltration Membranes: Investigation of Metal Ion Separations. *Desalination* **2011**, *267*, 57−63.
(31) Li, D.; McHugh, M. A. Limited Polysulfone Solubility in Supercritical Dimethyl Ether with THF and DMF Cosolvents. *J. Supercrit. Fluids* **2004**, *28*, 79−83.
(32) Wang, L.; Ding, H.; Shi, Y.; Liu, B. Effect of Diluent Mixture on Porous Structure of Polyphenylene Sulfide via Thermally Induced Phase Separation. *J. Macromol. Sci., Part A: Pure Appl. Chem.* **2009**, *46*, 1122−1127.
(33) van de Witte, P.; Dijkstra, P. L.; van den Berg, J. W. A.; Feijen, J. Phase Separation Processes in Polymer Solutions in Relation to Membrane Formation. *J. Membr. Sci.* **1996**, *117*, 1−31.
(34) Ulbricht, M. Advanced Functional Polymer Membranes. *Polymer* **2006**, *47*, 2217−2262.
(35) (a) Caneba, G. T.; Soong, D. S. Polymer Membrane Formation through the Thermal-Inversion Process. 1. Experimental Study of Membrane Structure Formation. *Macromolecules* **1985**, *18*, 2538−2545. (b) Caneba, G. T.; Soong, D. S. Polymer Membrane Formation through the Thermal-Inversion Process. 2. Mathematical Modeling of Membrane Structure Formation. *Macromolecules* **1985**, *18*, 2545−2555.
(36) Lloyd, D. R.; Kinzer, K. E.; Tseng, H. S. Microporous Membrane Formation via Thermally Induced Phase Separation. I. Solid-Liquid Phase Separation. *J. Membr. Sci.* **1990**, *52*, 239−261.
(37) Lloyd, D. R.; Kim, S. S.; Kinzer, K. E. Microporous Membrane Formation via Thermally-Induced Phase Separation. II. Liquid-Liquid Phase Separation. *J. Membr. Sci.* **1991**, *64*, 1−11.
(38) Kim, S. S.; Lloyd, D. R. Microporous Membrane Formation via Thermally-Induced Phase Separation. III. Effect of Thermodynamic Interactions on the Structure of Isotactic Polypropylene Membranes. *J. Membr. Sci.* **1991**, *64*, 13−29.
(39) Chan, P. K. Effect of Concentration Gradient on the Thermal-Induced Phase Separation Phenomenon in Polymer Solutions. *Modell. Simul. Mater. Sci. Eng.* **2006**, *14*, 41−51.
(40) Matsuyama, H.; Kudari, S.; Kiyofuji, H.; Kitamura, Y. Kinetic Studies of Thermally Induced Phase Separation in Polymer−Diluent System. *J. Appl. Polym. Sci.* **2000**, *76*, 1028−1036.
(41) Soroko, I.; Pessoa Lopes, M.; Livingston, A. The Effect of Membrane Formation Parameters on Performance of Polyimide Membranes for Organic Solvent Nanofiltration (OSN): Part A. Effect of Polymer/Solvent/Non-Solvent System Choice. *J. Membr. Sci.* **2011**, *381*, 152−162.
(42) (a) Yavea, W.; Quijada, R.; Serafini, D.; Lloyd, D. R. Effect of the Polypropylene Type on Polymer−Diluent Phase Diagrams and Membrane Structure in Membranes Formed via the TIPS Process. Part I. Metallocene and Ziegler−Natta Polypropylenes. *J. Membr. Sci.* **2005**, *263*, 146−153. (b) Yavea, W.; Quijada, R.; Serafini, D.; Lloyd, D. R. Effect of the Polypropylene Type on Polymer−Diluent Phase Diagrams and Membrane Structure in Membranes Formed via the TIPS Process. Part II. Syndiotactic and Isotactic Polypropylenes Produced Using Metallocene Catalysts. *J. Membr. Sci.* **2005**, *263*, 154−159.
(43) Yavea, W.; Quijada, R.; Ulbricht, M.; Benavente, R. Syndiotactic Polypropylene as Potential Material for the Preparation of Porous Membranes via Thermally Induced Phase Separation (TIPS) Process. *Polymer* **2005**, *46*, 11582−11590.
(44) Vanegasa, M. E.; Quijada, R.; Serafini, D. Microporous Membranes Prepared via Thermally Induced Phase Separation from Metallocenic Syndiotactic Polypropylenes. *Polymer* **2009**, *50*, 2081−2086.
(45) Atkinson, P. M.; Lloyd, D. R. Anisotropic Flat Sheet Membrane Formation via TIPS: Atmospheric Convection and Polymer Molecular Weight Effects. *J. Membr. Sci.* **2000**, *175*, 225−238.
(46) Matsuyama, H.; Maki, T.; Teramoto, M.; Asano, K. Effect of Polypropylene Molecular Weight on Porous Membrane Formation by Thermally Induced Phase Separation. *J. Membr. Sci.* **2002**, *204*, 323−328.
(47) Guo, B. H.; Fan, J. S.; Liu, J. D.; Xu, J.; Wang, X. L. Effect of Polypropylene Molecular Weight on Microporous Membrane Formation via Thermally Induced Phase Separation. *Acta Polym. Sin.* **2009**, *1*, 35−39.
(48) Tao, Y.; Yu, G.; Wang, X.; Wang, Z. Microporous Membranes Based on Electroconducting Polymers. *Int. J. Polym. Mater. Polym. Biomater.* **2011**, *60*, 706−719.
(49) Svec, F. Preparation and HPLC Applications of Rigid Macroporous Organic Polymer Monoliths. *J. Sep. Sci.* **2004**, *27*, 747−766.
(50) Ghasem, N.; Al-Marzouqi, M.; Duidar, A. Effect of PVDF Concentration on the Morphology and Performance of Hollow Fiber Membrane Employed as Gas−Liquid Membrane Contactor for CO_2 Absorption. *Sep. Purif. Technol.* **2012**, *98*, 174−185.
(51) Barton, A. F. M. *Handbook of Solubility Parameters and Other Cohesion Parameters*; CRC Press: Boca Raton, FL, 1983; pp 142−149.
(52) Yang, M.-C.; Perng, J.-S. Effect of Quenching Temperature on the Morphology and Separation Properties of Polypropylene Microporous Tubular Membranes via Thermally Induced Phase Separation. *J. Polym. Res.* **1998**, *5*, 213−219.
(53) Matsuyama, H.; Teramoto, M.; Kudari, S.; Kitamura, Y. Effect of Diluents on Membrane Formation via Thermally Induced Phase Separation. *J. Appl. Polym. Sci.* **2001**, *82*, 169−177.
(54) Yeow, M. L.; Liu, Y. T.; Li, K. Morphological Study of Poly(vinylidene fluoride) Asymmetric Membranes: Effects of the Solvent, Additive, and Dope Temperature. *J. Appl. Polym. Sci.* **2004**, *92*, 1782−1789.
(55) Cao, Y.; Croll, T. I.; O'Connor, A. J.; Stevens, G. W.; Cooper-White, J. J. Systematic Selection of Solvents for the Fabrication of 3D Combined Macro- and Microporous Polymeric Scaffolds for Soft Tissue Engineering. *J. Biomater. Sci., Polym. Ed.* **2006**, *17*, 369−402.
(56) Yang, J.; Wang, X.-L.; Tian, Y.; Lin, Y.; Tian, F. Morphologies and Crystalline Forms of Polyvinylidene Fluoride Membranes Prepared in Different Diluents by Thermally Induced Phase Separation. *J. Polym. Sci., Part B: Polym. Phys.* **2010**, *48*, 2468−2475.
(57) Lin, D.-J.; Beltsios, K.; Young, T.-H.; Jeng, Y.-S.; Cheng, L.-P. Strong Effect of Precursor Preparation on the Morphology of Semicrystalline Phase Inversion Poly(vinylidene fluoride) Membranes. *J. Membr. Sci.* **2006**, *274*, 64−72.
(58) Wang, X.; Wang, X.; Zhang, L.; An, Q.; Chen, H. Morphology and Formation Mechanism of Poly(vinylidene fluoride) Membranes Prepared with Immerse Precipitation: Effect of Dissolving Temperature. *J. Macromol. Sci., Part B: Phys.* **2009**, *48*, 696−709.
(59) Li, C.-L.; Wang, D.-M.; Deratani, A.; Quémener, D.; Bouyere, D.; Lai, J.-Y. Insight into the Preparation of Poly(vinylidene fluoride) Membranes by Vapor-Induced Phase Separation. *J. Membr. Sci.* **2010**, *361*, 154−166.
(60) Ahmad, A. L.; Ideris, N.; Ooi, B. S.; Low, S. C.; Ismail, A. Morphology and Polymorph Study of a Polyvinylidenefluoride (PVDF) Membrane for Protein Binding: Effect of the Dissolving Temperature. *Desalination* **2011**, *278*, 318−324.

(61) Ghasem, N.; Al-Marzouqi, M.; Rahim, N. A. Effect of Polymer Extrusion Temperature on Poly(vinylidene fluoride) Hollow Fiber Membranes: Properties and Performance Used as Gas−Liquid Membrane Contactor for CO_2 Absorption. *Sep. Purif. Technol.* **2012**, *99*, 91−103.
(62) Wang, X.; Yue, X.; Wang, X.; Guo, Q. Morphology, Crystallization and Formation Mechanism of Poly(vinylidene fluoride) Membranes Prepared with Immersion Precipitation: Effect of Maturation Time. *J. Macromol. Sci., Part B: Phys.* **2011**, *50*, 880−889.
(63) Lin, Y.; Tang, Y.; Ma, H.; Yang, J.; Tian, Y.; Ma, W.; Wang, X. Formation of a Bicontinuous Structure Membrane of Polyvinylidene Fluoride in Diphenyl Carbonate Diluent via Thermally Induced Phase Separation. *J. Appl. Polym. Sci.* **2009**, *114*, 1523−1528.
(64) Nakatsuka, K.; Ohmukai, Y.; Maruyama, T.; Matsuyama, H. Analysis of Solidification Rate of Polymer Solutions during PVDF Membrane Fabrication via TIPS Method. *Desalin. Water Treat.* **2010**, *17*, 275−280.
(65) Ghasem, N.; Al-Marzouqi, M.; Duaidar, A. Effect of Quenching Temperature on the Performance of Poly(vinylidene fluoride) Microporous Hollow Fiber Membranes Fabricated via Thermally Induced Phase Separation Technique on the Removal of CO_2 from CO_2-Gas Mixture. *Int. J. Greenhouse Gas Control* **2011**, *5*, 1550−1558.
(66) Matsuyama, H.; Berghmans, S.; Batarseh, M. T.; Lloyd, D. R. Effects of Thermal History on Anisotropic and Asymmetric Membranes Formed by Thermally Induced Phase Separation. *J. Membr. Sci.* **1998**, *142*, 27−42.
(67) Yoo, S. H.; Kim, C. K. Effects of the Diluent Mixing Ratio and Conditions of the Thermally Induced Phase-Separation Process on the Pore Size of Microporous Polyethylene Membranes. *J. Appl. Polym. Sci.* **2008**, *108*, 3154−3162.
(68) Ma, W.; Chen, S.; Zhang, J.; Wang, X. Kinetics of Thermally Induced Phase Separation in the PVDF Blend/Methyl Salicylate System and Its Effect on Membrane Structures. *J. Macromol. Sci., Part B: Phys.* **2010**, *50*, 1−15.
(69) Castro, A. J. Methods for Making Microporous Products. U.S. Patent 4,247,498, 1981.
(70) Brunauer, S.; Emmett, P. H.; Teller, E. Adsorption of Gases in Multimolecular Layers. *J. Am. Chem. Soc.* **1938**, *60*, 309−319.
(71) Barrett, E. P.; Joyner, L. G.; Halenda, P. P. The Determination of Pore Volume and Area Distributions in Porous Substances. I. Computations from Nitrogen Isotherms. *J. Am. Chem. Soc.* **1951**, *73*, 373−380.
(72) Hildebrand, J. H.; Scott, R. P. Solutions of Nonelectrolytes. *Annu. Rev. Phys. Chem.* **1950**, *1*, 75−92.
(73) Li, D.; Krantz, W. B.; Greenberg, A. R.; Sani, R. L. Membrane Formation via Thermally Induced Phase Separation (TIPS): Model Development and Validation. *J. Membr. Sci.* **2006**, *279*, 50−60.
(74) (a) Huggins, M. L. Solutions of Long Chain Compounds. *J. Chem. Phys.* **1941**, *9*, 440. (b) Flory, P. J. Thermodynamics of High Polymer Solutions. *J. Chem. Phys.* **1941**, *9*, 660−661. (c) Flory, P. J. *Principles of Polymer Chemistry*; Cornell University Press: Ithaca, NY, 1953; pp 495−518.
(75) (a) Hansen, C. M.; Skaarup, K. The Three Dimensional Solubility Parameter—Key to Paint Component Affinities. III. Independent Calculation of the Parameter Components. *J. Paint Technol.* **1967**, *39*, 511−514. (b) Hansen, C. M. *The Three Dimensional Solubility Parameter and Solvent Diffusion Coefficient—Their Importance in Surface Coating Formulation*; Danish Technical Press: Copenhagen, Denmark, 1967.
(76) Hansen, C. M. The Universality of the Solubility Parameter. *Ind. Eng. Chem. Prod. Res. Dev.* **1969**, *8*, 2−11.
(77) Hansen, C. M. *Hansen Solubility Parameters: A User's Handbook*, 2nd ed.; CRC Press: Boca Raton, FL, 2007.
(78) Barton, A. F. M. Applications of Solubility Parameters and Other Cohesion Parameters in Polymer Science and Technology. *Pure Appl. Chem.* **1985**, *57*, 905−912.
(79) Göltner, W. In *Modern Polyesters: Chemistry and Technology of Polyesters and Copolyesters*; Scheirs, J., Long, T. E., Eds.; John Wiley & Sons: Chichester, U.K., 2003; Chapter 13, pp 435−493.
(80) Nikles, D. E.; Farahat, M. S. New Motivation for the Depolymerization Products Derived from Poly(ethylene terephthalate) (PET) Waste: A Review. *Macromol. Mater. Eng.* **2005**, *290*, 13−30.
(81) Miller-Chou, B. A.; Koenig, J. L. A Review of Polymer Dissolution. *Prog. Polym. Sci.* **2003**, *28*, 1223−1270.
(82) Rouquerol, J.; Rouquerol, F.; Sing, K. S. W. *Adsorption by Powders and Porous Solids: Principles, Methodology and Applications*; Academic Press: San Diego, CA, 1999.
(83) McMullan, D. Scanning Electron Microscopy 1928−1965. *Scanning* **1995**, *17*, 175−185.
(84) Stevens, M. P. *Polymer Chemistry: An Introduction*, 3rd ed.; Oxford University Press: New York, 1999; p 143.
(85) Silverstein, M. S. PolyHIPEs: Recent Advances in Emulsion-Templated Porous Polymers. *Prog. Polym. Sci.* **2014**, *39*, 199−234.
(86) Robello, D. R.; Ulman, A.; Urankar, E. J. Poly(p-Phenylene Sulfone). *Macromolecules* **1993**, *26*, 6718−6721.
(87) Cytec Surface Specialties SA/NV. CYTEC Santosol Dimethyl Esters—Properties and Uses. Publication No. 230110E, version B; Brussels, Belgium (date unknown).
(88) Xiang, H. W.; Laesecke, A.; Huber, M. L. A New Reference Correlation for the Viscosity of Methanol. *J. Phys. Chem. Ref. Data* **2006**, *35*, 1597−1620 Table 5.